Author Accepted Manuscript. This article is published in Phys. Status Solidi B 2019, 256, 1800278,
https://doi.org/10.1002/pssb.201800278

The role of the Fe/Mo cations ordering degree and oxygen non-stoichiometry on the formation of the crystalline and magnetic structure of $Sr_2FeMoO_{6-\delta}$

Nikolay Kalanda, Vitalii Turchenko, Dmitry Karpinsky, Sergey Demyanov, Marta Yarmolich, Maria Balasoiu, Nicoleta Lupu, Sergey Tyutyunnikov, Nikolai A. Sobolev*

Dr. N.A. Kalanda*, Dr. D.V. Karpinsky, Prof. S.E. Demyanov, Dr. M.V. Yarmolich
Scientific-Practical Materials Research Centre of the NAS of Belarus, 220072 Minsk, Belarus

Dr. V.A. Turchenko
I.M. Frank Laboratory of Neutron Physics, Joint Institute for Nuclear Research, 141980 Dubna, Russia,
A.A. Galkin Donetsk Institute for Physics and Engineering, 83114 Donetsk, Ukraine

Dr. M. Balasoiu
I.M. Frank Laboratory of Neutron Physics, Joint Institute for Nuclear Research, 141980 Dubna, Russia,
Horia Hulubei National Institute for Physics and Nuclear Engineering, Bucharest, Romania,

Dr. N. Lupu
National Institute of Research and Development for Technical Physics, Iasi, Romania

Prof. S.I. Tyutyunnikov
V.I. Veksler and A.M. Baldin Laboratory of High Energy Physics, Joint Institute for Nuclear Research, 141980 Dubna, Russia

Prof. N.A. Sobolev
Departamento de Física and I3N, Universidade de Aveiro, 3810-193 Aveiro, Portugal,
National University of Science and Technology MISiS, 119049 Moscow, Russia

* Corresponding author. *E-Mail: kalanda@physics.by*

Keywords: strontium ferromolybdate, superstructural ordering, oxygen non-stoichiometry, neutron diffraction, magnetization

Single-phase $Sr_2FeMoO_{6-\delta}$ powders with various oxygen indices (δ) and degrees of the superstructural ordering (P) of the Fe/Mo cations were obtained from $SrFeO_{2.52}$ and $SrMoO_4$ reagents via solid-state synthesis. It has been established by means of the x-ray and neutron diffraction that, upon reducing the oxygen content and enhancing the superstructural ordering, the lengths of the Fe–O1 and Mo–O2 bonds in the crystal lattice increase, whereas the Fe–O2 and Mo–O1 bond lengths decrease. At the same time, the volume of the unit cell is reduced, which indicates an enhancement of the covalency degree of the bonds and stimulates a redistribution of the electron density, as well as an increase of the concentration of the spin-down charge carriers located in the conduction band on the Mo(t_{2g})↓ orbitals. This circumstance leads to an increase of the density of states at the Fermi level, accompanied by an amplification of the exchange interaction and elevation of the Curie temperature, which points to the leading role of the spin-polarized charge carriers at the Fermi level in the exchange interaction.

1. Introduction

The strontium ferromolybdate $Sr_2FeMoO_{6-\delta}$ (SFMO) with a double perovskite structure is a promising electronic material for the development of nonvolative magnetoresistive random-access memories (MRAM), reading heads for hard disks, high-sensitivity magnetic field sensors and fuel-cell electrodes [1-3]. For these applications, structurally perfect SFMO samples are needed which exhibit high values of the Curie temperature (T_C), saturation magnetization (M_s), degree of superstructural ordering (P) of the Fe/Mo cations and spin polarization of the free (delocalized) electrons [4-7].

An important problem in the microelectronic industry remains the improvement of the fabrication technology of high-quality, structurally perfect SFMO samples with reproducible magnetic and electrical transport properties. One of the most important preconditions of the maximal spin polarization in strontium ferromolybdate is the superstructural ordering of the Fe and Mo cations which sit in the centers of octahedrons, in whose apices the oxygen anions O(1) and O(2) are located [1, 2]. In the ideal picture, the Fe and Mo are alternatively placed in the structure surrounded by oxygen (superstructural ordering of the iron and molybdenum cations). However, some disorder between the two cations can occur, which means that two Fe atoms or Mo can sit next to each other [8]. It can be easily understood that anti-site disorder (ASD) affects the transport and magnetic properties as the overlapping of orbitals would be altered according to the degree of ASD. For example, the ASD degree plays a role on the Curie temperature [9] and the magnetoresistance [10]. In the absence of point defects, the ideal structure exhibits a long-chain superstructural ordering (P) of the cations $–Fe^{3+}–O^{2–}–Mo^{5+}–$ with high values of the saturation

magnetic moment (m_s) being close to the theoretical value 4.0 μ_B/f.u. In real crystals, various kinds of zero-dimensional defects, especially the Mo_{Fe}, Fe_{Mo} antisites and oxygen vacancies V_O, induce a distortion of the crystal structure, which leads to a redistribution of the electron density and to the formation of iron and molybdenum cations, $Fe^{2+}(3d^6)$ $\{S = 2\}$ and $Mo^{6+}(4d^0)$ $\{S = 0\}$, respectively. Diamagnetic $Mo^{6+}(4d^0)$ ions do not participate in the exchange interactions, and the latter ones between the $Fe^{2+}(3d^6)$ or $Fe^{3+}(3d^5)$ ions are necessarily negative, thus producing an antiferromagnetic ordering of the magnetic moments [11, 12]. Therefore, the distortion of the crystal lattice caused by defects in the cation and anion sublattices strongly influences the magnetic and electrical transport properties of strontium ferromolybdate [13-15].

It is known that the critical temperature (T_C) of the paramagnetic-ferrimagnetic transition, the saturation magnetization (M_s) and the electrical resistivity (ρ) are determined by the density of the electronic states $N(E)$ close to the Fermi level (E_F). In its turn, the $N(E)$ value depends on the oxygen concentration ($6–\delta$) and ordering of both antisite Mo_{Fe}, Fe_{Mo} defects and oxygen vacancies in the SFMO structure [5-7]. However, the functional dependence $\delta = f([Mo_{Fe}], [Fe_{Mo}])$ is not unique and is determined by the variation dynamics of both the oxygen nonstoichiometry and antisite defect concentration as a function of the SFMO synthesis regime (temperature T, duration t and partial oxygen pressure $p(O_2)$), because one and the same δ value can be obtained for different $[Mo_{Fe}]$, $[Fe_{Mo}]$ values, and vice versa [16, 17]. This circumstance leads to a situation in which several publications report different magnetic and electrical transport properties of SFMO samples prepared by similar methods [3-5]. One of the main reasons why these materials obtained under similar regimes are not widely used is a low reproducibility of their physical-chemical parameters. This fact indicates a high sensitivity of the compound to the synthesis parameters which affect the variation of δ and P values from sample to sample [6-14].

Thus, the motivation of the present work is rooted in the necessity to establish a correlation between the oxygen nonstoichiometry and the degree of superstructural ordering of the iron and molybdenum cations in SFMO with the aim of obtaining samples possessing optimum magnetic and electrical transport characteristics.

2. Experimental Section

Polycrystalline $Sr_2FeMoO_{6-\delta}$ samples were prepared by the solid-state synthesis technique from the $SrFeO_{2.52}$ (SFO) and $SrMoO_4$ (SMO) precursors. The latter were obtained by the standard ceramic technology from high-purity MoO_3, Fe_2O_3 oxides and strontium carbonate $SrCO_3$. Grinding and mixing of a stoichiometric blend of the starting components were carried out for 3 h in ethylalcohol in a vibromill. The obtained powders were dried at 350 K and then pressed into pellets. Upon the synthesis of the SFO and SMO precursors, the preliminary annealing was carried out for

20–40 h at 970 K and 1070 K, respectively. To increase the homogeneity of the batch, a repeated milling was used. The final synthesis of the SFO and SMO compounds was performed in an Ar atmosphere at $p(O_2) = 0.21 \cdot 10^5$ Pa at $T = 1470$ K for 20 h and 40 h, respectively, with a subsequent quenching down to room temperature. Then SFMO samples with different δ and P parameter values were obtained by means of annealing at 1420 K in a flux of the 5%H_2/Ar gas mixture for 20 h (sample A–1, $Sr_2FeMoO_{5.97}$, $P = 76\%$), 50 h (A–2, $Sr_2FeMoO_{5.94}$, $P = 86\%$) or 90 h (A–3, $Sr_2FeMoO_{5.94}$, $P = 93\%$).

The oxygen content in $SrFeO_{3-x}$ was determined by means of weighing the samples before and after their complete reduction in a hydrogen flux at 1373 K for 20 h resulting in the simple SrO oxide and Fe metal. The obtained strontium ferrite had the composition $SrFeO_{2.52}$. The 4–5 mm thick pellets with a diameter of 10 mm, consisting of the starting reagents $SrFeO_{2.52}$ and $SrMoO_4$ and having a stoichiometric composition, were annealed in a flux of the 5%H_2/Ar gas mixture at 1420 K for 5 h with a subsequent quenching to room temperature. The oxygen content in $Sr_2FeMoO_{6-\delta}$ was determined in the same way as in $SrFeO_{3-x}$.

The phase composition and crystal lattice parameters of the solid-state synthesis products were determined by the x-ray diffraction (XRD) analysis of the CuKα radiation in a DRON-3 diffractometer using the ICSD-PDF2 (Release 2000) database and the PowderCell [18], FullProf [19] software applying the Rietveld refinement technique. The diffraction curves were measured at room temperature at a scanning speed of 60º/h in the angular range $2\Theta =$ 10–90º. The degree of superstructural ordering of the iron and molybdenum cations (P) was calculated from the superstructure peaks ((101) and (103)) using the formula $P = (2 \cdot SOF - 1) \cdot 100\%$, where SOF is the site occupation factor calculated basing on the XRD data.

In order to study the crystalline and magnetic structure of $Sr_2FeMoO_{6-\delta}$, neutron diffraction measurements were performed at 300 K and 450 K in the high-resolution Fourier diffractometer (HRFD) based on the IBR-2 reactor in the Frank Laboratory of Neutron Physics of the Joint Institute for Nuclear Research (Dubna, Russia). A correlation technique of data accumulation was used at the HRFD, which provided a high resolution ($\Delta d/d \approx 0.001$, with d being the interplanar distance and Δd, the respective measurement error) that only weakly depends on the interplanar distance in a wide variation range of the latter. The high-resolution neutronograms were measured by detectors placed at mean neutron scattering angles of ± 152º in a range of the interplanar distances from 0.6 Å to 3.6 Å. The neutron diffraction data were analyzed by means of the FullProf software package [19] applying the Rietveld refinement technique.

The Curie temperature was determined through the analysis of the temperature dependences of the magnetization of the Sr2FeMoO6–δ samples by the ponderomotive technique in the temperature range from 77–800 K in an applied magnetic field of 0.86 T.

The electrical properties of the SFMO samples were studied using a multipurpose measurement system (Cryogenic Ltd.). The samples for these measurements had a rectangular shape with dimensions of 10×3×3 mm3. The electrical resistivity measurements were performed by a common four-point probe in the 4.2–600 K temperature range. To exclude parasitic thermo-EMF, the directions of the field and current were swapped.

3. Results and discussion

The crystal structure of SFMO is analogous to that of the ideal perovskite ABO_3 [1]. In contrast to ABO_3, the unit cell of the strontium ferromolybdate is characterized by the space group $\sqrt{2}\boldsymbol{a}_p \cdot \sqrt{2}\boldsymbol{a}_p \cdot 2\boldsymbol{a}_p$, where $\boldsymbol{a}_p$ is the parameter of the ideal perovskite lattice.

According to the x-ray phase analysis, the single-phase SFMO samples were obtained. The presence of the (101) and (103) reflexes indicates the appearance of the superstructural ordering of the iron and molybdenum cations in the SFMO unit cell (**Figure 1**).

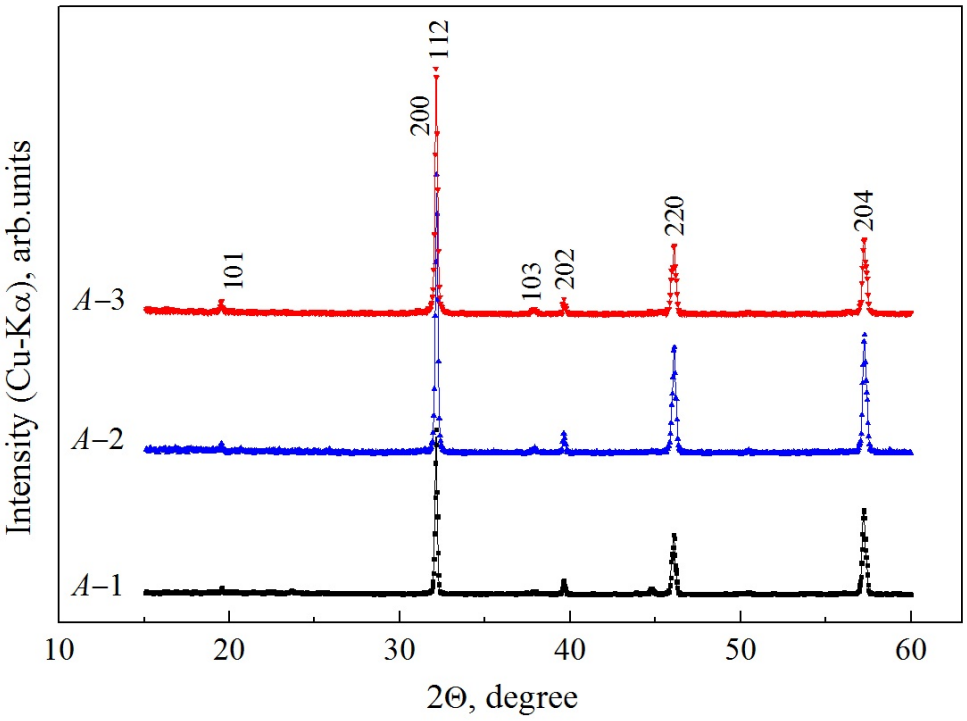

Figure 1 (color online). X-ray diffractograms of samples *A*–1, *A*–2 and *A*–3.

The results of the neutron diffraction measurements confirmed the single-phase composition of all samples. At temperatures below T_C they have a tetragonal symmetry of the unit cell (space group *I4/mmm*), and above T_C they are characterized by the cubic $Fm\bar{3}m$ symmetry group. The analysis of the neutron diffraction data permitted a more precise determination of the oxygen content in the samples. Samples *A*–1 and *A*–2 had different oxygen indices δ, whereas the δ values for samples *A*–2 and *A*–3 were practically equal.

The neutron diffraction measurements for samples *A*–1 and *A*–2, performed at room temperature and refined using the Rietveld method, are presented in **Figure 2**.

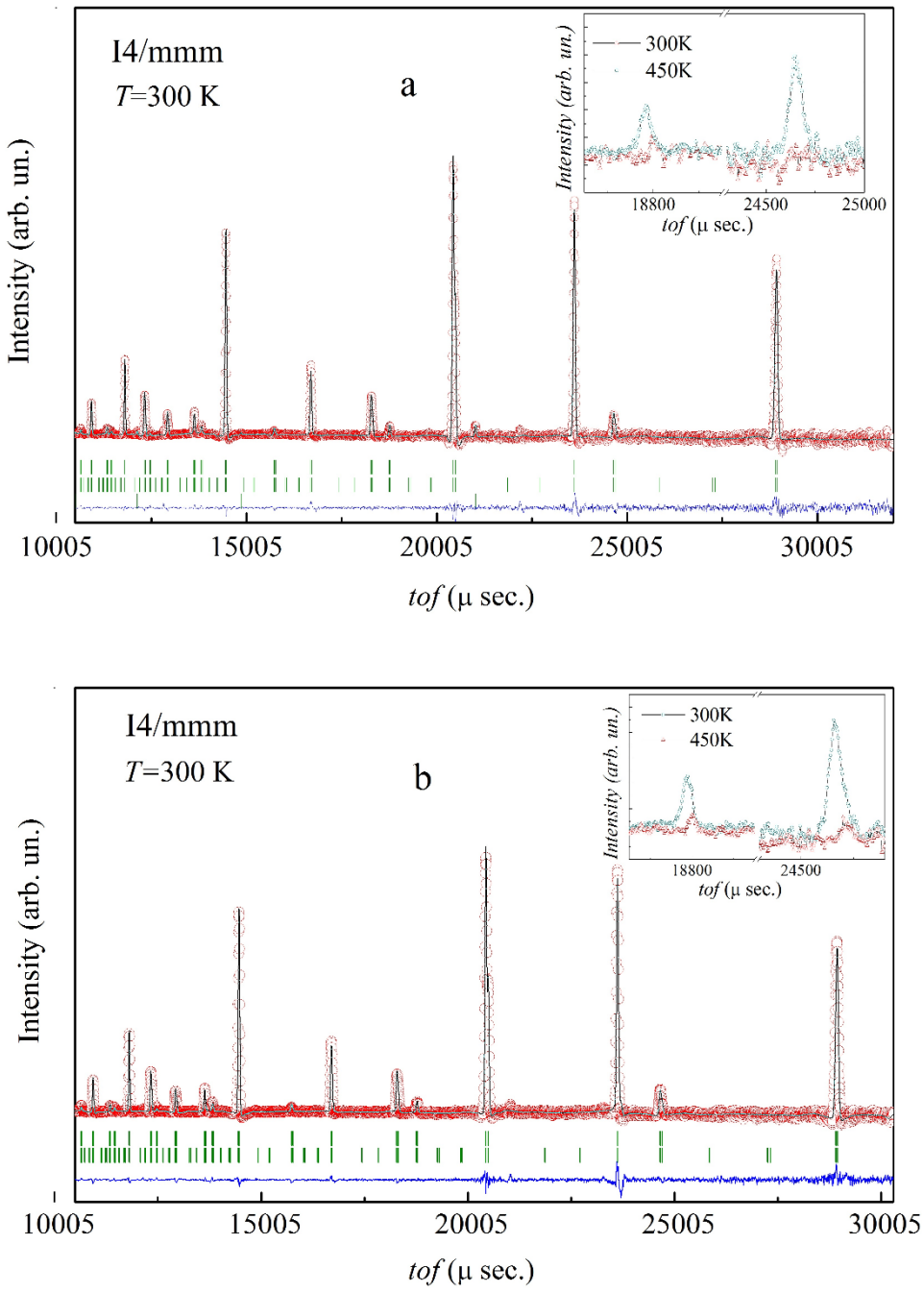

Figure 2 (color online). Neutron diffraction patterns of the samples *A*–1 (a) and *A*–2 (b) taken at room temperature. The evolution of the reflexes, corresponding to the magnetic phase, at temperatures varying from 300 K to 450 K, is shown in the insets.

According to the neutron diffraction data obtained at room temperature, the Fe and Mo atoms occupy the 2a and 2b positions in the SFMO structure, have the coordination number N = 6 and are enclosed in the octahedron formed by the O(1) and O(2) oxygen atoms. Through the analysis of the

neutron diffraction data, an influence of the oxygen index δ and the superstructural ordering degree P of the Fe/Mo cations on the bond lengths between the molybdenum, iron and oxygen ions Mo–O и Fe–O has been concluded (Table 1).

The values of the reliability factors (Rwp < 15% и $1 < \chi 2 < 2$) shown in Table 1 attest a high degree of concordance between the experimental and theoretical data, which allowed a sufficiently precise determination of the unit cell parameters, bond lengths and coordinates of the ions.

On the assumption of the equality of the bonding energy of the O(1) and O(2) anions with the crystal lattice and according to the results of Refs. [20-23], the oxygen vacancies may be formed both in the basis plane (Fe/Mo–O(2)) and along the OZ axis in the Fe/Mo–O(1) planes. Therefore, with increasing δ, a growth of both the a and c parameters should be expected, which corresponds to an increase of the bond lengths and thus to an increase of the unit cell volume.

However, we have found that the a and c parameter weakly decrease with increasing concentration of the anion vacancies and superstructural ordering degree of the Fe/Mo cations. It has been established that the Fe–O(1) bonds shorten and the Mo–O(1) ones lengthen, which witnesses to a compression of the FeO6 octahedron and a stretching of the MoO6 octahedron along the OZ axis. At the same time, the unit cell volume slightly diminishes, which indicates an enhancement of the bond covalency due to a stronger overlap of the cation and anion orbitals (Figure 3). It occurs because the superstructural ordering of the Fe/Mo cations has a stronger influence on the variation of the crystal lattice parameters than the oxygen deficiency.

Table 1. Lattice parameters (a, c) and reduced volumes of unit cells (for the tetragonal phase $V_{red} = V/4$ and for the cubic phase $V_{red} = V/8$), atomic positions, metal-oxygen bond lengths, isotropic Debye-Waller factors (B_{iso}) and agreement factors (R_{wp}, R_{exp}, R_B, R_{mag}, χ^2) in SFMO as determined at various temperatures using the Rietveld refinement, were R_{wp} is the Weighted Profile Factor, R_{exp} is the Expected Weighted Profile Factor, R_B the is Bragg Factor, R_{mag} is the magnetic Rietveld factor, χ^2 is the reduced chi-square [18, 19].

Composition	*A*–1 *T*=300 K *(I4/mmm)*	*A*–1 *T*=450 K *(Fm$\bar{3}$m)*	*A*–2 *T* =300 K *(I4/mmm)*	*A*–2 *T*=450 K *(Fm$\bar{3}$m)*	*A*–3 *T*=300 K *(I4/mmm)*	*A*–3 *T*=450 K *(Fm$\bar{3}$m)*
***a* (Å)**	5.5770(4)	7.9059(1)	5.5788(3)	7.9055(3)	5.5746(2)	7.9055(1)
***c* (Å)**	7.9074(6)	—	7.9067(4)	—	7.9070(3)	—
V_{red}(Å^3)	61.48 (3)	61.76 (1)	61.46 (2)	61.75 (3)	61.42(6)	61.75 (1)
O1	4*e* (0,0,*z*)	24*e*	4*e* (0,0,*z*)	24*e*	4*e* (0,0,*z*)	24*e* (*x*,0,0)
z*/*c	0.2507(8)	0.2518(7)	0.24945(5)	0.2519(7)	0.2488(5)	0.2525(8)
O2	8h (*x*,*x*,0)	—	8h (*x*,*x*,0)	—	8h(*x*,*x*,0)	
x*/*a	0.2493(6)	—	0.2503(3)	—	0.2507(8)	
Fe – O1	1.9830	1.9907	1.9726	1.9919	1.9670	1.9967
Fe – O2	1.661		1.9737		1.9764	
Mo – O1	1.9707	1.9907	1.9813	1.9919	1.9860	1.9967
Mo – O2	1.9775		1.9690		1.9655	
B_{iso}, Å^2	0.826(19)	—	0.832(15)	—	0.2599(4)	—
R_{wp}, %	9.59	9.13	9.83	9.62	10.4	12.3
R_{exp}, %	7.00	6.36	6.98	6.88	7.56	9.10
R_B, %	3.09	2.71	4.10	3.34	3.87	6.26
R_{mag}, %	13.9	—	11.4	—	8.67	—
χ^2	1.87	1.99	1.98	1.96	1.88	1.83

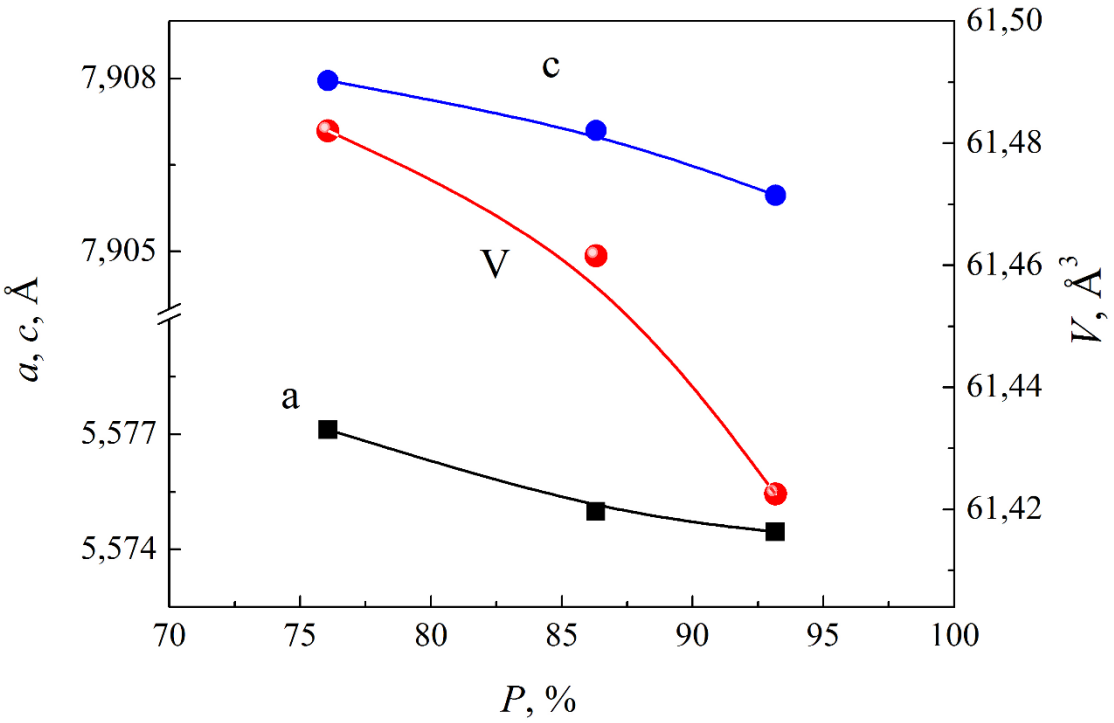

Figure 3. Crystal lattice parameters and unit cell volume of Sr2FeMoO6–δ vs. the superstructural ordering degree of the Fe/Mo cations at T = 300 K.

Figure 4 shows the (001) and (100) planes of the tetragonal unit cell which contain oxygen ions located at different structural positions, O1 (4e) and O2 (8h), which allows estimating the charge density distribution for all possible Mo(Fe)–O ion pairs. This distribution was calculated by means of the Vesta/Venus software package using the maximal entropy approach [24].

The unit cell parameters, ion coordinates and populations, calculated from the XRD patterns of sample A–3 at room temperature, were used as input data. The obtained results point to a shift of the charge density distribution toward the molybdenum ions along the Fe–O(1)–Mo и Fe–O(2)–Mo chains, which applies to all investigated compositions. To a great extent, this shift occurs due to a higher electronegativity of the molybdenum ions as compared to the iron ones. The redistribution of the electron density along the Fe–O(1)–Mo and Fe–O(2)–Mo chains promotes an increase of the concentration of spin-down-polarized electrons located in the conduction band at the Mo(t2g)↓ orbitals.

a) b)

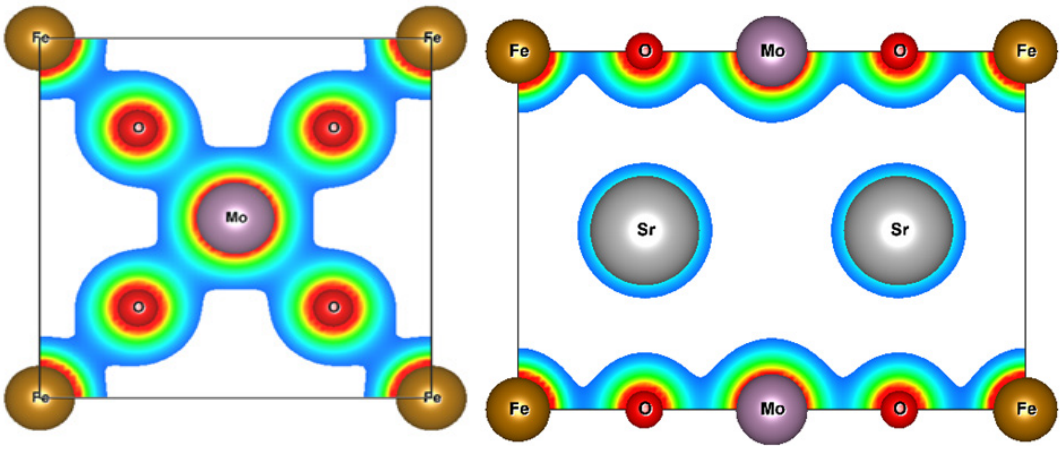

Figure 4 (color online). Visualization of the charge density in sample A–3 in the (001) (a) and (100) (b) planes containing the O2 and O1 oxygen anions, respectively.

The results obtained by means of the Vesta/Venus software package [24] using the maximal entropy approach agree well with the experimental measurements of the electrical conductivity of samples A–1, A–2 and A–3, see Figure 5. As all these samples exhibit a metallic conduction, one may use the classical Drude formula:

$$\rho = 1 / N(EF) \cdot e2 \cdot \upsilon F2 \cdot \tau, \qquad (1)$$

where N(EF) is the density of spin-polarized carriers at the Fermi level, e the electron charge, υF the electron velocity at the Fermi level, τ (T) the mean linear momentum relaxation time of the charge carriers. The factor N(EF), being determined by the density of states at the Fermi level, can only increase upon a rise of the superstructural ordering degree of the Fe/Mo cations which depends on the population of the oxygen sites (O(1) и O(2)). When the unit cell volume decreases (Figure 3), the bond covalency in the Fe – O – Mo chains increases, which enhances the degree of the overlap of the electron wavefunctions. In the case of the metallic conduction and at a fixed temperature, the terms υF (T) and τ (T) are constant, so that according to Equation 1 the diminution of ρ is caused by a rise of N(EF).

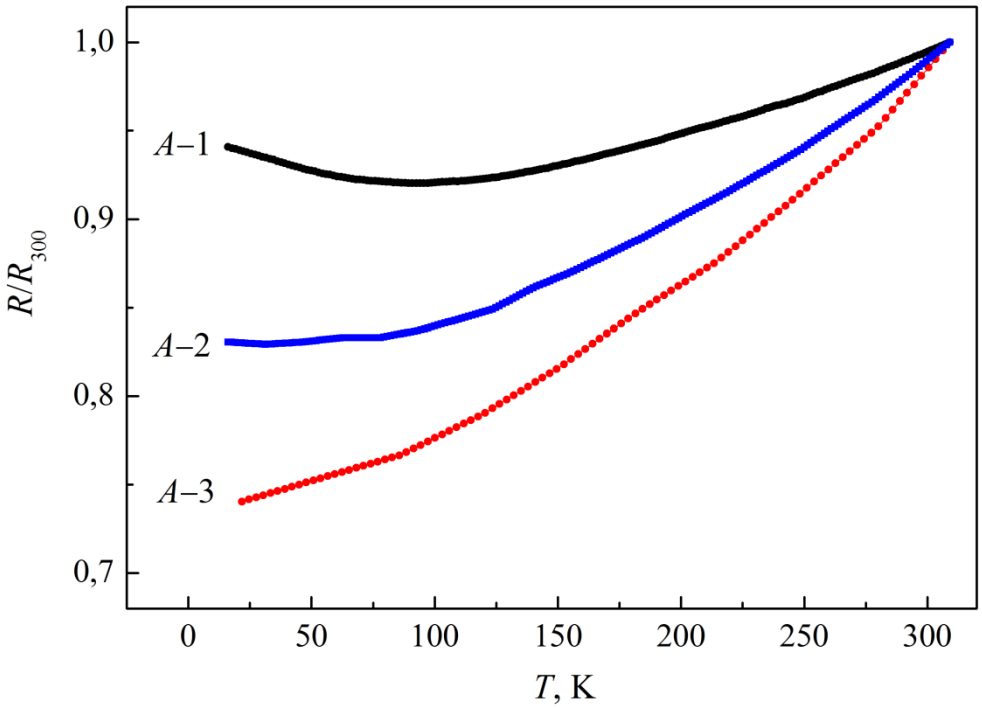

Figure 5 (color online). Experimentally measured temperature dependence of the normalized electrical resistance of the $Sr_2FeMoO_{6-\delta}$ samples.

Besides, we have found out that an increase of P is accompanied by a rise of the magnetization $M(T)$ values in the temperature range from 77 K to T_C, and at 77 K they amount to $M(A–1)_{77K}$ = 26.41 $A \cdot m^2 \cdot kg^{-1}$, $M(A–2)_{77K}$ = 32.36 $A \cdot m^2 \cdot kg^{-1}$ and $M(A–3)_{77K}$ = 42.66 $A \cdot m^2 \cdot kg^{-1}$ (**Figure 6**). It has also been established that samples A–1, A–2, A–3 have temperatures of the paramagnetic-ferrimagnetic transitions amounting to $T_C \approx$ 422 K, $T_C \approx$ 428 K и $T_C \approx$ 437 K, respectively. The monotonous growth of T_C with increasing P correlates also with the diminution of the electrical resistivity of the investigated samples and, respectively, with a rise of the spin-polarized charge carrier concentration. This fact indicates that the spin-polarized charge carriers at the Fermi level have a dominating role on the exchange interactions, which corroborates the conclusions drawn by other authors [25-29].

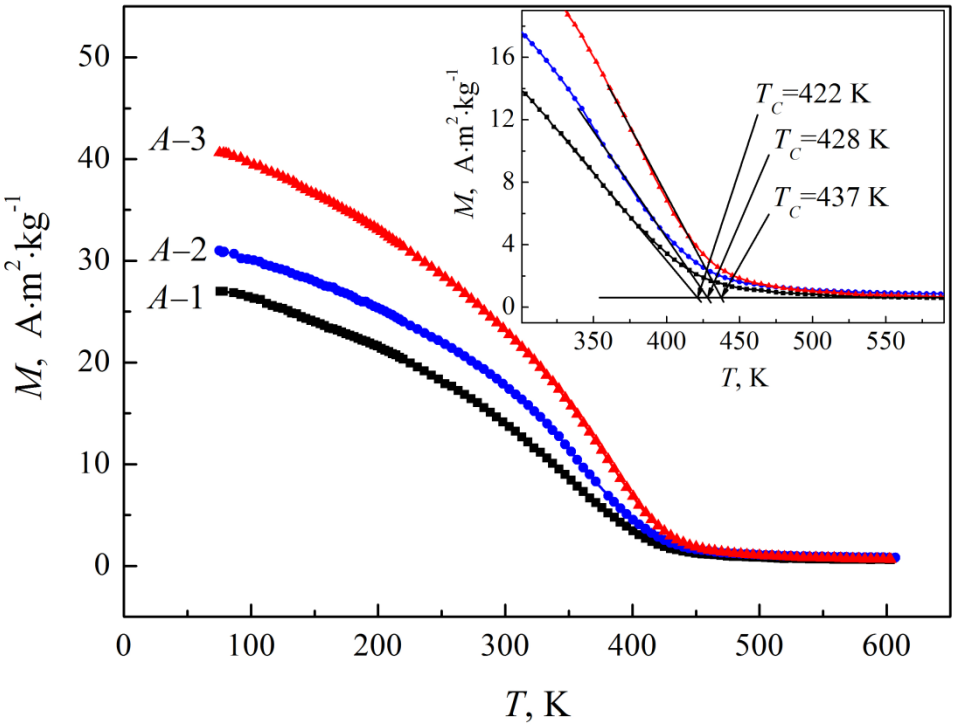

Figure 6 (color online). Temperature dependence of the magnetization of samples *A*–1, *A*–2 and *A*–3, measured in the applied magnetic field $B = 0.86$ T. The inset represents the temperature dependence of the magnetization on a increased scale.

Some authors have suggested that the exchange interaction between the iron and molybdenum cations in the double perovskite occurs according to the Zener double exchange mechanism, as it is the case in manganites [27, 30-33]. Tovar *et al.* [34] argue that the exchange interaction is realized through free spin-polarized electrons after the Ruderman – Kittel – Kasuya – Iosida (RKKI) mechanism [30, 31]. We are also inclined to this interpretation because, according to the RKKI theory, an increase of the free carrier concentration leads to a rise of the density of states at the Fermi level and, as a consequence, to an enhancement of the exchange interaction and to a rise of the Curie temperature. Sarma *et al.* [35, 36] affirmed that the double exchange does not take place in SFMO because the Fe(3d)↑ orbitals are completely occupied and the spin-down (↓) electrons can only occupy the Fe(t_{2g})↓ levels, thus becoming delocalized. As a result, electron-electron interaction between the delocalized spin-down electrons on the Mo($4d^1$) orbitals and the localized spin-up Fe($3d^5$) electrons according to Hund's law cannot occur. However, this is fundamentally necessary for the double exchange. Hence, the latter appears improbable in SFMO.

As it follows from the obtained data, the growth of T_C and reduction of ρ are a consequence of a rise of the oxygen vacancy concentration leading to an increase of the oxygen non-stoichiometry from $\delta = 0.03$ to $\delta = 0.06$ (**Figures 5, 6**). According to the XRD measurements (**Figure 1**), it has been concluded that the oxygen deficiency induces the superstructural ordering of

the Fe/Mo cations, diminution of the chemical bond length and unit cell volume, thus enhancing the overlap of the electron orbitals accompanied by the formation of a long-chain Fe–O–Mo ordering, as well as promoting an increase of the spin-polarized charge carrier concentration at the Fermi level on the hybridized Fe($3d_{t2g}$)-O(2p)-Mo($4d_{t2g}$) orbitals.

4. Conclusions

By means of the neutron diffraction data we have revealed the variation tendency of the Mo–O and Fe–O bond lengths in SFMO as a function of the oxygen deficiency index δ and the superstructural ordering degree P of the Fe/Mo cations. It has been established that the O1–Fe/Mo–O1 and O2–Fe/Mo–O2 bond lengths along the (001) and (110) crystallographic planes shorten, thus leading to a reduction of the unit cell volume. This tendency indicates an enhancement of the bond covalency, which stimulates a redistribution of the electron density and increases the concentration of the spin-down electrons located in the conduction band on the Mo(t_{2g})↓ orbitals. These data permit us to assume that the exchange interaction in SFMO is realized through free spin-polarized electrons according to the RKKI mechanism.

Acknowledgements

The work has been supported by the European project H2020-MSCA-RISE-2017-778308 – SPINMULTIFILM, as well as by the FCT of Portugal through the project I3N/FSCOSD (Ref. FCT UID/CTM/50025/2013).

References

[1] D. Serrate, J.M.De Teresa, M.R. Ibarra. J. Phys.: Condens. Matter. **2007**, *19*, 023201.

[2] D. Topwal, D.D. Sarma, H. Kato, Y. Tokura, M. Avignon. Phys. Rev. B. **2006**, *73*, 0944191.

[3] M. Kalanda, G. Suchaneck, A.M. Saad, S. Demyanov, G. Gerlach. Mater. Sci. Forum. **2010**, *636-637*, 338.

[4] K.-I. Kobayashi, T. Kimura, H. Sawada, K. Terakura, Y. Tokura. Nature **1998**, *395*, 677.

[5] T.-Y. Cai, S. Ju, Z.-Y. Li. Condens. Matter. **2006**, *18*, 11347.

[6] N. Kalanda, S. Demyanov, W. Masselink, A. Mogilatenko, M. Chashnikova, N. Sobolev, O. Fedosenko. Cryst. Res. Technol. **2011**, *46*, 463.

[7] R. Allub, O. Navarro, M. Avignon, B. Alascio. Physica B: Condens. Matter. **2002**, *320*, 13.

[8] A. S. Ogale, S. B. Ogale, R. Ramesh, T. Venkatesan, Appl. Phys. Lett. **1999**, *75*, 537.

[9] J. Navarro, J. Nogues, J. S. Munoz, J. Fontcuberta, Phys. Rev. B. **2003**, *67*, 174416.

[10] D. Niebieskikwiat, F. Prado, A. Caneiro, R. D. Sanchez, Phys. Rev. B. **2004**, *70*, 132412.

[11] Y. Zhang, V. Ji, K.-W. Xu. J. Alloys Compd. **2015**, *648*, 374.

[12] A. M. Reyes, Y. Arredondo, O. Navarro. J. Phys. Chem. C. **2016**, *120*, 4048.

[13] J. Rager, M. Zipperle, A. Sharma, J. L. MacManus-Driscoll. J. Am. Ceram. Soc. **2004**, *87*, 1330.

[14] J. P. Zhou, R. Dass, H.Q. Yin, J.-S. Zhou, L. Rabenberg, J.B. Goodenough. J. Appl. Phys. **2000**, *87***,** 5037

[15] Q. Zhang, Z.F. Xu, L.F. Wang, S.H. Gao, S.J. Yuan. J. Alloys Compd. **2015**, *649*, 1151.

[16] H. Wu, Y. Ma, Y. Qian, E. Kan, R. Lu, Y. Liu, W. Tan, C. Xiao , K. Deng. Solid State Commun. **2014**, *177*, 57.

[17] M. Saloaro, M. Hoffmann, W. A. Adeagbo, S. Granroth, H. Deniz, H. Palonen, H. Huhtinen, S. Majumdar, P. Laukkanen, W. Hergert, A. Ernst, P. Paturi. ACS Appl. Mater. Interfaces. **2016**, *8*, 20440.

[18] J. Rodríguez-Carvajal. Commission on powder diffraction (IUCr). Newsletter. **2001**, *26*, 12.

[19] W. Kraus, G. Nolze. J. Appl. Crystallogr. **1996**, *29*, 301.

[20] R. Kircheisen, J. Topfer. J. Solid State Chem. **2012**, *185*, 76.

[21] S. Agata, Y. Moritomo, A. Machida, K. Kato A. Nakamura. Jpn. J. Appl. Phys. **2002**, *41*, L688.

[22] S. Nakayama, T. Nakagawa, S. Nomura. J. Phys. Soc. Jpn. **1968**, *24*, 219.

[23] N. Menéndez, M. García-Hernández, D. Sánchez, J. D. Tornero, J. L. Martínez, J. A. Alonso. Chem. Mater. **2004**, *16*, 3565.

[24] K. Momma and F. Izumi. J. Appl. Cryst. **2011**, *44*, 1272.

[25] M. Retuerto, M.J. Martínez-Lope, M. García-Hernández, J.A. Alonso. Mater. Res. Bull. **2009**, *44*, 1261.

[26] B. Martinez, J. Navarro, L.I. Balcells, J. Fontcuberta. Phys.: Condens. Matter. **2000**, *12*, 10515.

[27] C. Ritter, M.R. Ibarra, L. Morellon, J. Blasco J. García, J. M. De Teresa. J. Phys.: Condens. Matter. **2000**, *12*, 8295.

[28] N.A. Kalanda, S.E. Demyanov, A.V. Petrov, D.V. Karpinsky, M.V. Yarmolich, S.K. Oh, S.C. Yu, D.–H. Kim. J. Electron. Mater. **2016**, *45*, 3466.

[29] M. Yarmolich, N. Kalanda, S. Demyanov, Ju. Fedotova, V. Bayev, N. Sobolev. Phys. Status Solidi B. **2016**, *253*, 2160.

[30] M. Besse, V. Cros, A. Barthélémy, H. Jaffrès, J. Vogel, F. Petroff, A. Mirone, A. Tagliaferri, P. Bencok, P. Decorse, P. Berthet, Z. Szotek, W.M. Temmerman, S.S. Dhesi, N.B. Brookes, A. Rogalev, A. Fert. Europhys. Lett. **2002**, *60*, 608.

[31] J. Lindén, T. Yamamoto, M. Karppinen, H. Yamauchi. Appl. Phys. Lett. **2000**, *76*, 2925.

[32] L. dos Santos-Gómeza, L. León-Reinab, J.M. Porras-Vázquezc, E. R. Losillaa, D. Marrero-López. Solid State Ionics. **2013**, *239*, 1.

[33] J.B. Goodenough. Magnetism and the chemical bond. Wiley, New York-London, **1963**.

[34] M. Tovar, M.T. Causa, A. Butera, J. Navarro, B. Martinez, J. Fontcuberta, M.C.G. Passeggi. Phys. Rev. B. **2002**, *66*, 024409.

[35] D.D. Sarma, Curr. Opin. Solid State Mater. Sci. **2001**, *5*, 261.

[36] D.D. Sarma, P. Mahadevan, T. Saha-Dasgupta, S. Ray, and A. Kumar, Phys. Rev. Lett. **2000**, *85*, 2549.